2013 IEEE/RSJ International Conference on
Intelligent Robots and Systems (IROS)
November 3-7, 2013. Tokyo, Japan

Caging Complex Objects with Geodesic Balls

Dmitry Zarubin Florian T. Pokorny Marc Toussaint Danica Kragic

***Abstract*— This paper proposes a novel approach for the synthesis of grasps of objects whose geometry can be observed only in the presence of noise. We focus in particular on the problem of generating caging grasps with a realistic robot hand simulation and show that our method can generate such grasps even on complex objects. We introduce the idea of using geodesic balls on the object's surface in order to approximate the maximal contact surface between a robotic hand and an object. We define two types of heuristics which extract information from approximate geodesic balls in order to identify areas on an object that can likely be used to generate a caging grasp. Our heuristics are based on two scoring functions. The first uses winding angles measuring how much a geodesic ball on the surface winds around a dominant axis, while the second explores using the total discrete Gaussian curvature of a geodesic ball to rank potential caging postures. We evaluate our approach with respect to variations in hand kinematics, for a selection of complex real-world objects and with respect to its robustness to noise.**

I. Introduction

A popular approach for grasp synthesis in robotics is based on *local contact-level techniques*. Given friction coefficients and an accurate mesh-representation of the object, these methods use a grasp quality scoring function Q (*e.g.* as in [1]) defined in terms of contact points and surface normals on the object to generate force-closure grasps. The main drawbacks of these methods are that one needs to know friction coefficients and they typically do not degrade gracefully in the presence of noise since even a small amount of noise in the vertex positions of a mesh can result in large deviations of the estimated normal vectors.

In this work, we study the problem of synthesizing caging grasps. Such grasps do not necessarily establish contact with the object, but force the object to remain within a bounded distance from the robot hand. While caging grasps have so far mainly been studied using analytic methods for simple polygonal objects in 2D, we contribute by providing a new heuristic synthesis algorithm for such grasps which is applicable to complex 3D objects. The contributions of this paper can be summarized as follows:

- We introduce the idea of using geodesic balls on an object's surface to approximate the contact surface between a hand and an object.

Dmitry Zarubin and Marc Toussaint are with the Machine Learning and Robotics Lab, Universität Stuttgart, Stuttgart, Germany, {Dmitry.Zarubin,Marc.Toussaint}@ipvs.uni-stuttgart.de.

Florian T. Pokorny and Danica Kragic are with the Centre for Autonomous Systems, Computer Vision and Active Perception Lab, School of Computer Science and Communication, KTH Royal Institute of Technology, Stockholm, Sweden, {fpokorny, dani}@kth.se.

This work was supported by the EU FP7 project TOMSY (IST-FP7-270436).

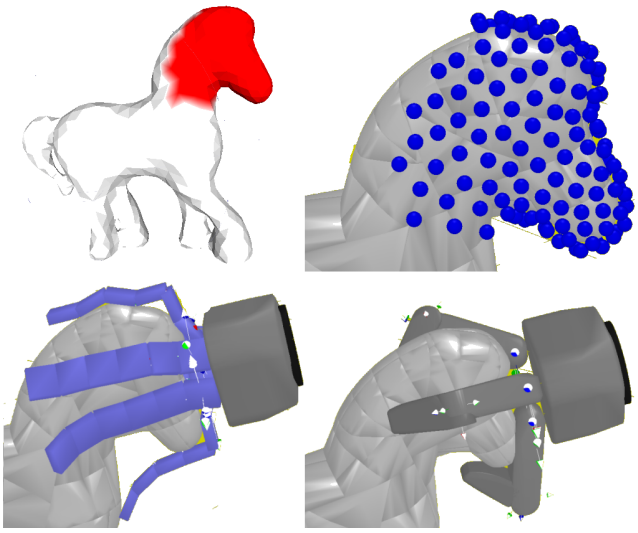

Fig. 1. An illustration of our curvature based sphere caging heuristic. The red area in the top left picture highlights an approximate geodesic ball on the surface with a large value of our discrete curvature integral. The three other plots demonstrate an application of our sphere caging heuristic. The manipulators used for the evaluation are: a net of points (upper right), a multi-joint 6 finger hand (lower left) and a 3-finger Schunk hand (lower right).

- We develop novel heuristics based on winding angles and discrete curvature integrals to select suitable grasp centre points for two types of caging grasps which we call circle and sphere caging. For *circle caging*, which is motivated by caging an object by a curve which is almost closed (as in Fig. 4), we develop a method for choosing appropriate grasping points using *winding angles*. For *sphere caging*, which is motivated by the idea of enclosing an object as much as possible by a geodesic ball, our approach is based on integrated discrete Gauss curvature.
- We evaluate our approach in simulation with respect to noise, for various objects and object sizes and for several hand kinematics: a deformable hand simulation by a net of points, a simulated multi-joint 6-finger hand and a 2-finger hand, a 3-finger Schunk hand and a 5-finger anthropomorphic hand.

Our paper is structured as follows: In Sections II and III, we review related literature and the notion of winding numbers and discrete curvature which we require later on. In Section IV, we present our approach towards the synthesis of caging grasps, while, in Section V, we discuss our experimental evaluation of this approach. Finally, we conclude our work in Section VI and discuss potential future directions.

II. Related work

Two major directions in grasping research are based on force-closure and caging respectively. In approaches using force closure grasps – that is grasps which can withstand external wrenches in arbitrary direction – a set of potential grasp hypotheses is usually ranked according to a scoring function measuring the 'goodness' of a grasp. Popular choices include the L^1 and L^∞ grasp quality functions defined in [1]. State of the art simulators such as GraspIT [2] and OpenGRASP [3] can be used to determine stable grasp configurations using random sampling or heuristics based approaches. An example of a sampling based approach is provided by the work of [4], and the recent work [5] integrates sampling with a suitable object representation and grasp ranking procedure. While the force closure condition can be easily evaluated once the local contact geometry is known, the concept of a *caging grasp* is more intricate since it can depend on the full *global geometry* of the object. Some of the earliest works considered the case of an object in the plane and defined it to be caged by a set of n points in the plane if the object could not be moved arbitrarily far away from these points [6]. An interesting work on the relation between grasping and caging is presented in [7]. There, a caging grasp is considered to provide a useful waypoint towards a stable force-closure grasp. In [8], the authors investigated caging grasps for the manipulation of articulated objects with handles such as doors and windows. Their approach generates a set of caging grasps on such handles which led to a greater success rate compared to a local contact based approach. In [9], a caging approach based on topological features of objects with holes is investigated.

A few papers such as [10] have used curvature-based features to identify grasping configurations. In [10], it is assumed that concave points of a 2D elliptic Fourier descriptor of an object are most suitable for grasping. Good grasping candidates are preselected by means of curvature extrema and then evaluated further using the concept of force-closure. Another related work [11] proposes a grasping algorithm for unknown 3D objects. There, Gaussian curvature is employed during the segmentation of the object. The labelling of sub-parts of the object is then done with respect to neighbourhoods of extrema of Gaussian curvature. These works depend on the use of point-wise approximations of Gaussian curvature and are hence rather unstable under noise. While the robustness with respect to noise can be increased by an additional smoothing step, we shall take a different approach in our work since we will work with a discrete version of Gaussian curvature defined for any mesh.

III. Background

Let us consider a mesh M with vertex set $V(M)$ and where $F(v)$ denotes the set of faces containing vertex $v \in V(M)$. In this case, the total Gauss curvature $K(v)$ for a vertex $v \in V(M)$ is defined by $K(v) = 2\pi - \sum_{f \in F(v)} \theta(v, f)$ [12], where $\theta(v, f)$ denotes the angle of the face f at vertex v. The sign of $K(v)$ has the same interpretation as the sign of the usual Gaussian curvature, and points are called Euclidean, spherical or hyperbolic if $K(v) = 0$, $K(v) > 0$ or $K(v) < 0$ respectively [12]. Recall that the Gauss-Bonnet theorem for a smooth closed oriented surface $S \subset \mathbb{R}^3$ states that the integral of the standard Gaussian curvature satisfies $\int_S K \, \mathrm{dVol} = 2\pi\chi(S)$, where $\chi(S)$ denotes the Euler characteristic of S. The Euler characteristic $\chi(S)$ is a topological quantity which is invariant under certain continuous deformations of S (*i.e.* homotopies) and we have $\chi(S) = 2 - 2g$, where g is the genus of the surface. Interestingly, for a closed polyhedral surface $M \subset \mathbb{R}^3$, the Gauss-Bonnet theorem has a discrete analogue:

$$\sum_{v \in V(M)} K(v) = 2\pi\chi(M), \tag{III.1}$$

where the sum is over vertices in M and K now denotes the discrete total Gauss curvature. Further results in this direction are discussed in [12], [13]. While $K(v)$ shares some properties with the standard Gaussian curvature, another more closely related version of K which we shall not use in this work can be provided by normalizing $K(v)$ by the 'mixed area' around the vertex v (see [14] for details).

Let us now discuss winding numbers which we shall be inspired by to define our circle caging heuristic. We shall use a version of winding numbers for non-closed curves in order to measure the wrapping of a hand around an object. Our motivation is similar to [15] and [16] where concepts from topology such as *writhe* and *winding numbers* are used for grasping and character animation respectively. Recall that the winding number of a closed curve $\gamma : [0, 1] \to \mathbb{R}^2$ not containing the origin in $\mathbb{R}^2$ is an integer determining how many times γ 'wraps around the origin' with the sign being determined by the orientation of γ.

Definition III.1. Let $\gamma : [0, 1] \to \mathbb{R}^2$ be closed, smooth and suppose γ does not traverse the origin. Then the winding number $w(\gamma) \in \mathbb{Z}$ around the origin is given by

$$w(\gamma) = \frac{1}{2\pi}(\theta(1) - \theta(0)).$$

where $\gamma(t) = (r(t), \theta(t))$ in polar coordinates, and where r denotes the radial and θ the angular coordinate.

For a closed curve, the quantity $w(\gamma)$ is topological in nature and does not change under continuous deformations of γ not traversing the origin. If we apply the above formula – which is applicable also in the case of piece-wise linear curves – to non-closed curves, we obtain a measure for how γ wraps around the origin in a suitable coordinate system. Note however that this quantity for non-closed curves is not a topological invariant anymore.

IV. Methodology

Unlike the common caging approach of working with a planar scenario with fingers represented by points or discs such as in [17], we are interested in the synthesis of caging grasps in 3D, for a complex object and using a real robot hand. Since no analytic solution to the general caging grasp synthesis problem is currently known, we shall explore a heuristic approach which enables us to:

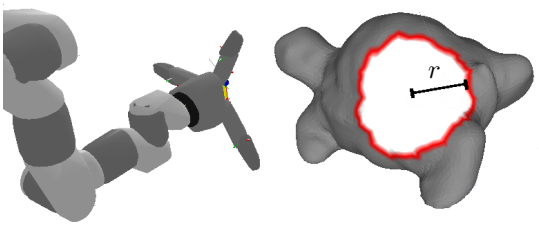

Fig. 2. We approximate the projection of the robot hand's surface onto the turtle object by a geodesic ball whose radius r is proportional to the robot hand's finger length.

a) synthesize likely caging grasp postures using information about the 'hand-local' geometry of an object
b) evaluate differing robot hand geometries for the purpose of generating caging grasps.

Our approach consists of three main parts: a suitable object mesh representation, a representation of the object/robot hand interaction and a quality scoring function for two types of caging heuristics which we call circle and sphere caging.

A. Object representation and preprocessing

We assume that we have a potentially noisy mesh representation M of an object of interest available. Such object meshes are used *e.g.* in the work of [18] and can be obtained using laser range or Kinect sensor data. Since we will be interested in efficiently computing approximate geodesic balls on M, and in order for our discrete curvature K to be distributed evenly across the mesh, we would like to work with a mesh with approximately equal triangle size. For this purpose, we chose isotropical remeshing as a pre-processing step. Isotropical remeshing preserves the shape of the surface and provides an almost equilateral triangulation. We start with an input mesh M and perform modifications using the tool [19] in three steps: a) oversampling and a sub-division is applied to M, b) vertices are uniformly resampled, c) the positions of the vertices are optimized using area equalization and Lloyd's relaxation method. The resulting triangle mesh then has almost equal edge lengths. We chose parameters so that the maximal deviation between edge-lengths was about 30% of the mean edge length, but this deviation can be significantly reduced further by increasing the number of triangles per mesh.

Another important part of the preprocessing is a convex decomposition of the object. The *PhysX Engine* [20] which we are using for realistic physical simulations requires all shapes to be convex in order to efficiently compute collisions. For this purpose, we used the convex decomposition library [21] and generated a decomposition of each object into approximately 100 convex meshes.

B. Representing the hand-object interaction

Common approaches towards the synthesis of both force-closed grasps and caging grasps simplify the geometry of the robot's hand by working only with a discrete number of contact points or caging points respectively [18], [17]. In this work, we propose to instead think about an approximation

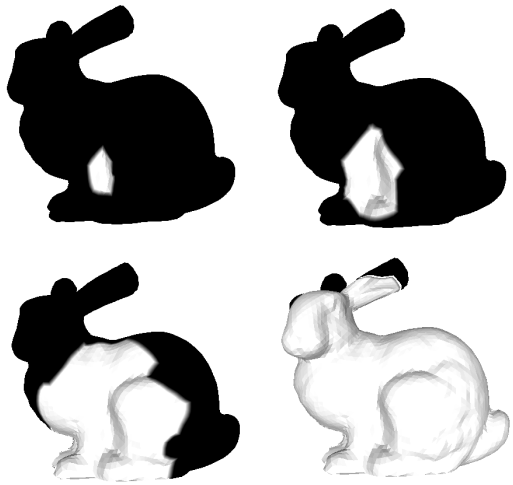

Fig. 3. Geodesic ball approximations $G_r(p)$ (coloured white) for a fixed vertex p and for radii r of increasing size on an isotropically remeshed bunny object. The size of the radius r corresponds to the finger-length of different robotic hands.

of the $2D$ *contact surface* that a robot hand can make with an object. We model the maximal contact surface between the robot's hand and a given closed surface S as a geodesic ball $B_r(p)$ of radius r and centred at a point $p \in S$. Such a geodesic ball then represents the 'hand-local' geometry of M for a robot hand whose fingers are approximately of length r. We think of $B_r(p)$ as a first order approximation of the projection of the robot's hand onto the object as visualized in Fig. 2. Since the calculation of an exact geodesic ball $B_r(p)$ is computationally challenging, we use the mesh M with vertex set V and consider a rough approximation of $B_r(p)$ by a sub-mesh $G_r(p) \subseteq M$ instead. Since all triangles in M are approximately equilateral, we use Dijkstra's algorithm to determine $G_r(p)$ as follows: we approximate the distance between two vertices $p, q \in V$ by calculating the number of vertices in the shortest edge-path between them and scaling the result by the mean edge length. $G_r(p)$ then denotes the submesh containing all triangles whose vertices are of distance at most r from p. Fig. 3 displays $G_r(p)$ for a fixed vertex p and for four different radii of increasing size. Since r varies with the size of the robotic hand, different geometric information is captured by $G_r(p)$ for differing hand size.

C. Circle and sphere caging

We propose two types of caging grasp heuristics which we call circle ($\mathbb{S}^1$) and sphere ($\mathbb{S}^2$) caging respectively. We introduce scoring functions which use our approximate geodesic balls $G_r(p)$ and which enable us to rank the likelihood of finding a caging grasps corresponding to one of these heuristics.

$\mathbb{S}^1$ *cages:* Here, we define a heuristic for caging an object with a curve $\gamma : [0,1] \to \mathbb{R}^3$ which wraps almost completely around an elongated part of an object such as the red curve in Fig. 4. We call this type of grasp an $\mathbb{S}^1$, or circle cage, since the curve γ is almost a closed circle in simple cases. Inspired by the notion of winding numbers for closed curves which we recalled in Def. III.1, we propose

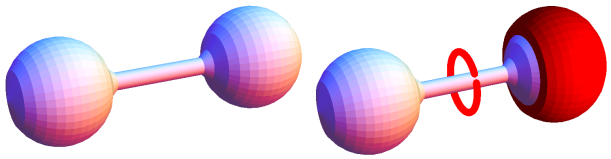

Fig. 4. Illustration of circle and sphere caging on a dumbbell object.

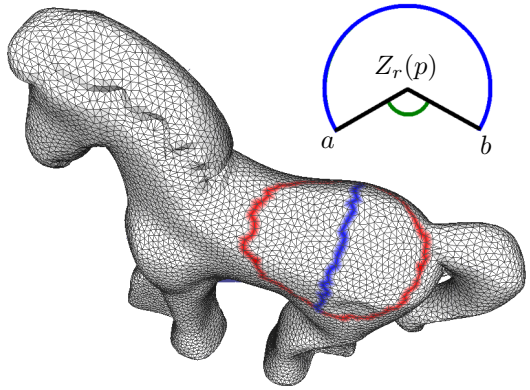

Fig. 5. Evaluating potential $\mathbb{S}^1$ cages: The blue line highlights vertices close to the plane $\Pi_r(p)$ for a fixed vertex p and orthogonal to the main axis $A_r(p)$ of the vertices lying on the depicted geodesic ball $G_r(p)$ with red border. The wrapping of $G_r(p)$ around the horse is approximated using the angles between the end-points of the blue curve around the central axis of $G_r(p)$. The upper right sketch illustrates the solid angle $Angle_{Z_r(p)}(a,b)$ (in green) between the centre of mass $Z_r(p)$ and the projections of the end-points of $P_r(p)$ onto $\Pi_r(p)$

a simple approach to quantify the winding of γ around the object: for each vertex p of our object mesh M, we compute a major axis $A_r(p)$ and centre of mass $Z_r(p)$ of the set of vertices of $G_r(p)$ and a plane $\Pi_r(p)$ through $Z_r(p)$ which is orthogonal to $A_r(p)$. We now compute an edge-path $P_r(p)$ in the object mesh approximating $\Pi_r(p) \cap G_r(p)$. Fig. 5 depicts an example of this calculation. To quantify the amount of winding of $P_r(p)$ around the object, we finally project the path $P_r(p)$ onto the plane $\Pi_r(p)$ and compute the winding angle $W_r(p) = 2\pi - Angle_{Z_r(p)}(a,b)$, where $Angle_{Z_r(p)}(a,b)$ denotes the solid angle between the centre of mass $Z_r(p)$ and the projections of the end-points of $P_r(p)$ onto $\Pi_r(p)$. $W_r(p)$ takes values in $[\pi, 2\pi]$. This quantity can be easily computed without having to represent the projection $\gamma : [0,1] \to \Pi_r(p)$ of the curve $P_r(p)$ in polar coordinates centred at $Z_r(p)$ as $\gamma(t) = (r(t), \theta(t))$. Furthermore, since for our purposes γ satisfies $\pi \leqslant |\theta(1) - \theta(0)| \leqslant 2\pi$ in all but degenerate cases, we opted to use the winding angle $W_r(p)$ to measure the amount of wrapping of γ around $Z_r(p)$.

We now propose to rank the vertices of our object mesh by the resulting winding angles $W_r(p)$, with high winding angles indicating a higher likelihood that the curve $P_r(p)$ yields an $\mathbb{S}^1$ caging grasp for the object. Let us now discuss a related concept of $\mathbb{S}^2$, or sphere caging, before connecting the above with the geometry of a robot hand and the actual synthesis of such cages.

$\mathbb{S}^2$ *cages:* Consider the case of an object-part which is almost completely enclosed by a geodesic ball such as the right part of the dumbbell object in Fig. 4 which is clearly caged by the red contact surface resembling a part of a sphere. Let us consider using the integrated total Gauss curvature on $G_r(p)$ as a heuristic for measuring how $G_r(p) \subseteq M$ wraps around the M, and recall that it equals $2\pi\chi(M)$ when $G_r(p)$ covers a closed mesh M completely. In this work, we hence evaluate whether geodesic balls with a large total curvature are good candidates for applying a caging grasp. We consider the scoring function S_r defined by

$$S_r(p) = \sum_{v \in V(G_r(p))} K(v),$$

where K denotes the total Gauss curvature introduced in Section III and where $V(G_r(p))$ denotes the vertex set of an approximate geodesic ball $G_r(p)$ on M. Since the total Gauss curvature does not distinguish convex and concave parts of the object and since we would prefer to grasp locally convex parts of the object, we furthermore exclude geodesic balls with centre vertices v which have a concave 1-ring neighbourhood in the mesh from further analysis.

D. Hand representation and positioning

We now relate the concepts of circle and sphere caging of curves and geodesic balls on an object mesh to the kinematics of a robot hand. For this purpose, we need to be able to define a correspondence between a pose of a robotic hand and an approximate geodesic ball $G_r(p)$ or the projection of the path $P_r(p)$ onto the plane $\Pi_r(p)$ respectively. In our experiments, which we shall describe later, we have tested several types of manipulators: an artificial net of small spheres distributed over an approximate geodesic ball, a simulated multi-joint 6 finger hand (for sphere caging), a multi-joint 2 finger hand (for circle caging), a realistic simulation of a 3 finger Schunk hand and a 5 finger anthropomorphic hand.

Caging with a net of points: As we already mentioned in previous sections, an important part of our method is a projection and approximation of a hand's contact surface by a geodesic ball. It is logical then to investigate the robustness of the approach if we had a robotic hand whose contact surface was very close to such a ball. The recently proposed Universal Gripper [22] is an example of a deformable hand coming close to this idealization. In our simulation, we generated a structure designed to imitate a soft robotic hand which makes a geodesic ball contact with the object. We created a small sphere for every vertex inside $G_r(p)$ and moved it along the normal direction by a fixed offset away from the object. Then, we gradually shifted all spheres back towards the object along the normal direction until a small threshold distance is achieved. For circle caging, we chose only those vertices on the mesh close to the path $P_r(p)$ and applied the same procedure to obtain spheres lying near $P_r(p)$ but outside the object. This procedure then simulates a contact surface obtained using a deformable robot hand and which is approximated by a net of points. Examples for both $\mathbb{S}^1$ and $\mathbb{S}^2$ cases are depicted in the second column of Fig. 8.

The 'hexapus' and the 2-finger hand: Here, we considered a multi-joint 6-finger hand which we created within the freely available robot simulator libORS [23]. Every finger consists

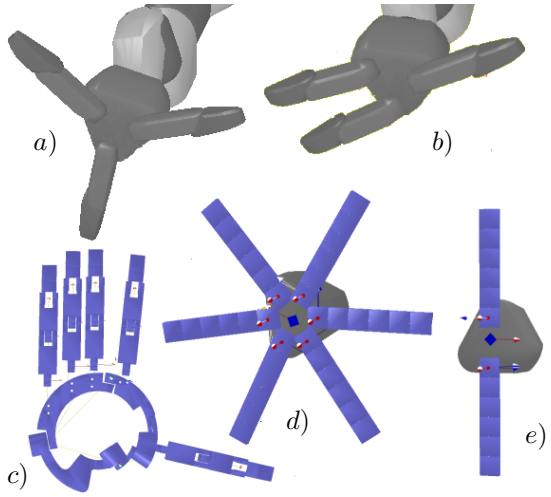

Fig. 6. The configuration of the robot hand before closing fingers for sphere a,d) and circle b,e) caging is displayed. The simulated anthropomorphic, multi-joint 6 and 2 finger hands c,d,e) have more degrees of freedom than the Schunk hand displayed in a,b).

of 6 square segments and is attached via a revolute joint to the hand base. This 'hexapus' hand structure is similar to biologically inspired soft robotic actuators described in [24] and [25]. We define the 2-finger hand displayed in Fig. 6e) by using only 2 opposing fingers of this 'hexapus' hand.

The Schunk hand: We implemented a simulation of the 7 degrees of freedom 3-finger Schunk hand commonly used in grasping applications (depicted in the top row in Fig. 6).

The anthropomorphic hand: We have further tested a 'human-like' hand in our experiments. Every finger of this metamorphic anthropomorphic hand developed in the laboratory of Prof. Jian S. Dai at KCL [26] consists of 3 segments. The reconfigurable palm allows for additional freedom of the thumb (as shown in Fig 6c).

Positioning and automatic closing of the hands: Recall that the radius of our approximate geodesic ball $G_r(p)$ is chosen to match the finger length of our robotic hands, so as to provide a possibility for the hand to cover such balls with an open palm posture (Fig. 2 and 6). Our grasp synthesis is implemented as follows: for a geodesic ball $G_r(p)$ that is *optimal* (has highest value) with respect to our scoring functions $W_r(p)$ or $S_r(p)$, the hand base is first placed at a certain distance from p along the surface normal direction. A suitable preshape as in the Fig. 6 is then adopted and the hand base orientation is set to be parallel to the surface and, for the circle caging case, the main axis along the stretched fingers is aligned orthogonal to the main axis of $G_r(p)$. The 'hexapus' hand is used only for $\mathbb{S}^2$ caging and the 2-finger hand only for $\mathbb{S}^1$ caging. For the anthropomorphic hand, we selected the same preshape for both $\mathbb{S}^1$ and $\mathbb{S}^2$ caging. Next, we gradually move the palm towards the surface until the distance to the surface reaches a small threshold, varying with the object size. In the final phase, we perform a standard autoclose procedure: we move the finger segments (starting from those closest to the palm) towards the object until the distance between each segment and the object is smaller than a fixed threshold value. This is done preserving the opposing finger configuration for the circle, and the equal angular spread between the fingers for the sphere caging case. For the net of points 'hand', we simply place the hand over the geodesic ball $G_r(p)$ as described in the previous section.

V. Simulation Experiments

Let us now describe a series of experiments which test several aspects of our circle and sphere caging heuristics: a) the general success rates of our approach and its robustness to noise, b) its dependence on object shape and size c) its applicability for various robot hand kinematics. We explain the methodological details of the experimental setup and present a success evaluation for our caging heuristics. Finally, we conclude with a qualitative discussion of several example cages. Our experimental setup is outlined in Alg. 1.

Algorithm 1 Evaluation algorithm

Require: original 3D model M, scale s, noise level σ
Ensure: stability analysis of cages for K noisy meshes
  for 1 to K **do**
    Remove all faces.
    Add uniform noise from $[-\sigma, \sigma]$ to every vertex.
    Reconstruct a new mesh using MeshLab package [27].
    Perform isotropical remeshing.
    Compute scoring functions according to section IV-C.
    Select best grasp centre point on the *noisy* mesh.
    Position and autoclose the hand on the *original* mesh.
    Test if the grasp is a caging grasp using *PhysX*.
  end for
  return % of successful caging grasps (robustness)

A. Evaluation methods

Simulation of perceptual noise: In practice, a triangulated 3D model of an object is constructed from noisy sensor data. In order to simulate perceptual noise on a synthetic object mesh, we perturbed every vertex of the original mesh by a uniformly distributed offset in $[-\sigma, \sigma]$ and reconstructed a new mesh from the vertex point cloud using the Poisson tool from the Meshlab package [27]. The actual value of the maximal offset σ used in simulations was chosen empirically to be equal to 1% of the bounding sphere radius. After isotropical remeshing, we then obtain a mesh with 1000 vertices. As a result of this process, the original mesh may differ significantly from the resulting noisy reconstructed mesh as shown in Fig. 7.

Physical simulation: We applied a realistic physics simulation using the PhysX software package to test if an object was successfully caged. After placing the hand and closing the fingers according to section IV-D, the object and the manipulator were copied to the physical environment with gravity and standard friction forces (the friction coefficient was set to 1). We simulated 10 consecutive random rotational motions of the manipulator 'in air' for 100 simulation steps each and deemed a grasp stable if the object was still within a small distance of the hand and had not fallen onto a simulated floor under the influence of gravity.

TABLE I

ROBUSTNESS OF CAGING HEURISTICS

Experiments			Robustness of sphere caging					Robustness of circle caging			
Objects	Scale	Curvature integral value, π	Net of points	Hexapus hand	Schunk hand	Anthropo-morphic hand	Winding value, π	Net of points	2-finger hand	Schunk hand	Anthropo-morphic hand
Dumbbells	1	4 ± 0	100%	100%	50%	60%	2 ± 0	100%	40%	90%	80%
Dumbbells	4	3 ± 0.16	100%	100%	100%	80%	2 ± 0	100%	90%	80%	100%
Dumbbells	8	0.89 ± 0.02	0%	0%	0%	0%	1.92 ± 0.04	90%	90%	40%	90%
Pony	1	-7.2 ± 1.6	100%	100%	80%	80%	2 ± 0	90%	20%	80%	70%
Pony	4	1.56 ± 0.12	90%	80%	20%	30%	2 ± 0	100%	90%	20%	70%
Pony	8	1.77 ± 0.04	0%	40%	0%	0%	1.98 ± 0.03	70%	40%	0%	30%
Cup	1	-2.36 ± 2.65	100%	100%	80%	60%	1.99 ± 0.01	90%	30%	30%	40%
Cup	4	1.27 ± 0.53	50%	10%	10%	40%	2 ± 0	90%	30%	10%	30%
Cup	8	0.70 ± 0.15	20%	60%	40%	70%	1.97 ± 0.04	60%	50%	10%	30%
Bunny	1	4 ± 0	100%	100%	80%	60%	2 ± 0	100%	80%	90%	80%
Bunny	3	2.58 ± 0.11	100%	100%	60%	40%	2 ± 0	100%	40%	0%	10%
Bunny	8	1.97 ± 0.04	20%	20%	30%	30%	1.90 ± 0.05	20%	20%	0%	10%

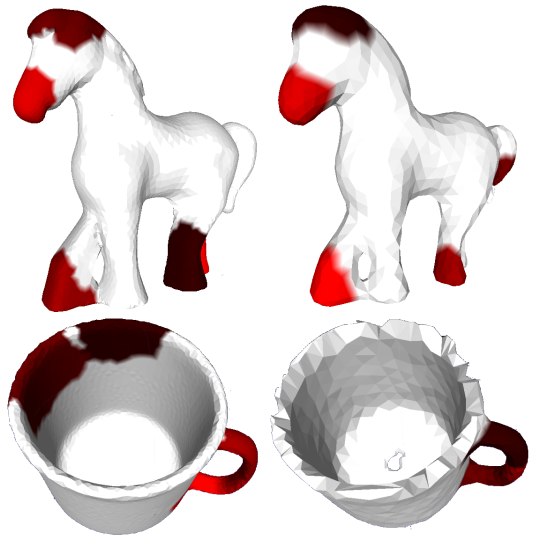

Fig. 7. The effect of additional noise on the original meshes (displayed on the left) is shown. For illustration purposes, we display five caging areas with highest scoring function values. The colour intensity increases with the value of W_r and S_r as indicated. Noisy meshes (right column) are generated from the original meshes (left column) by adding noise, reconstructing from a point cloud and remeshing according to methodological section IV-A. Two types of caging grasp scoring functions are presented: $\mathbb{S}^2$ for the pony object and $\mathbb{S}^1$ for the cup. Note that the highest scoring areas on the bottom right cup are overlapping around the handle.

Computational complexity: All experiments were done on a computer with an Intel i5, 4 Core, 2.40GHz processor with 4 GB memory. The computation time of our scoring functions scales in the worst case (small object size compared to r in $G_r(p)$) quadratically in the number of vertices. For small objects, the average computation time was about 20 seconds (1000 vertices per object), while the computation for medium and large objects took less than a second.

B. Evaluation of our $\mathbb{S}^1$ and $\mathbb{S}^2$ caging heuristic

We produced 10 synthetic noisy meshes with 1000 vertices according to the method outlined in the previous section for the dumbbells, pony, cup and bunny models depicted in Fig. 8. We tested three different object sizes with a scaling factor between 1 and 8. The scaling factor was computed as a ratio $\frac{R_b}{F_l}\pi$, where R_b is a bounding sphere radius and F_l the Schunk hand's finger length. A value of 1 for the scale of an object therefore represents an object size such that a full caging inside the robot hand is likely to be possible. Other scales were chosen empirically in order to represent medium (3-4) and large (8) scale objects. We followed Alg. 1 to evaluate our approach but used the same previously generated $K = 10$ noisy meshes per object for each scale and manipulator to speed up the experiments. Results are presented in Table I for sphere (left side) and circle caging (right side) respectively. The maximal integrated curvature and winding angles are given as multiples of π.

Manipulators: The net of points showed the best average success rate over all experiments and was the best on average for $\mathbb{S}^1$ caging (followed by the anthropomorphic hand) and second best (after the 'hexapus' hand) for $\mathbb{S}^2$ caging. The 3-finger Schunk hand demonstrates a high amount of variations in stability rates depending on the size and type of an object. For the latter hand, the object might simply slip out between fingers when small enough, whereas additional fingers and flexibility prevent this in case of the 'hexapus' and anthropomorphic hand which performed slightly better.

Scale: The smallest scale was selected, as explained above, to enable a full caging by a robot hand. Thus, the stability rate for the net of points or the 'hexapus' hand in this case is close to 100% with a few exceptions in the $\mathbb{S}^1$ case. For the medium size objects, the results are also good and demonstrate the ability of our method to select the most suitable subparts of an object. Large scale objects are mainly unstable and success in this case depends fully on the object's structure.

$\mathbb{S}^1$ and $\mathbb{S}^2$ caging: The total Gauss curvature integral for a closed polyhedral surface $M \subset \mathbb{R}^3$ equals $2\pi\chi(M)$ (see Eq. III.1). Furthermore, recall that $\chi(M) = 2 - 2g$ where g denotes the genus of M which is non-zero for the cup and pony objects. In the case of genus zero objects such as the bunny and the dumbbells, a good caging success rate seemed to occur if the integrated curvature over $G_r(p)$ was larger than 50% of the total (*i.e.* larger than 2π), but there was a substantial amount of variation between the robot hands.

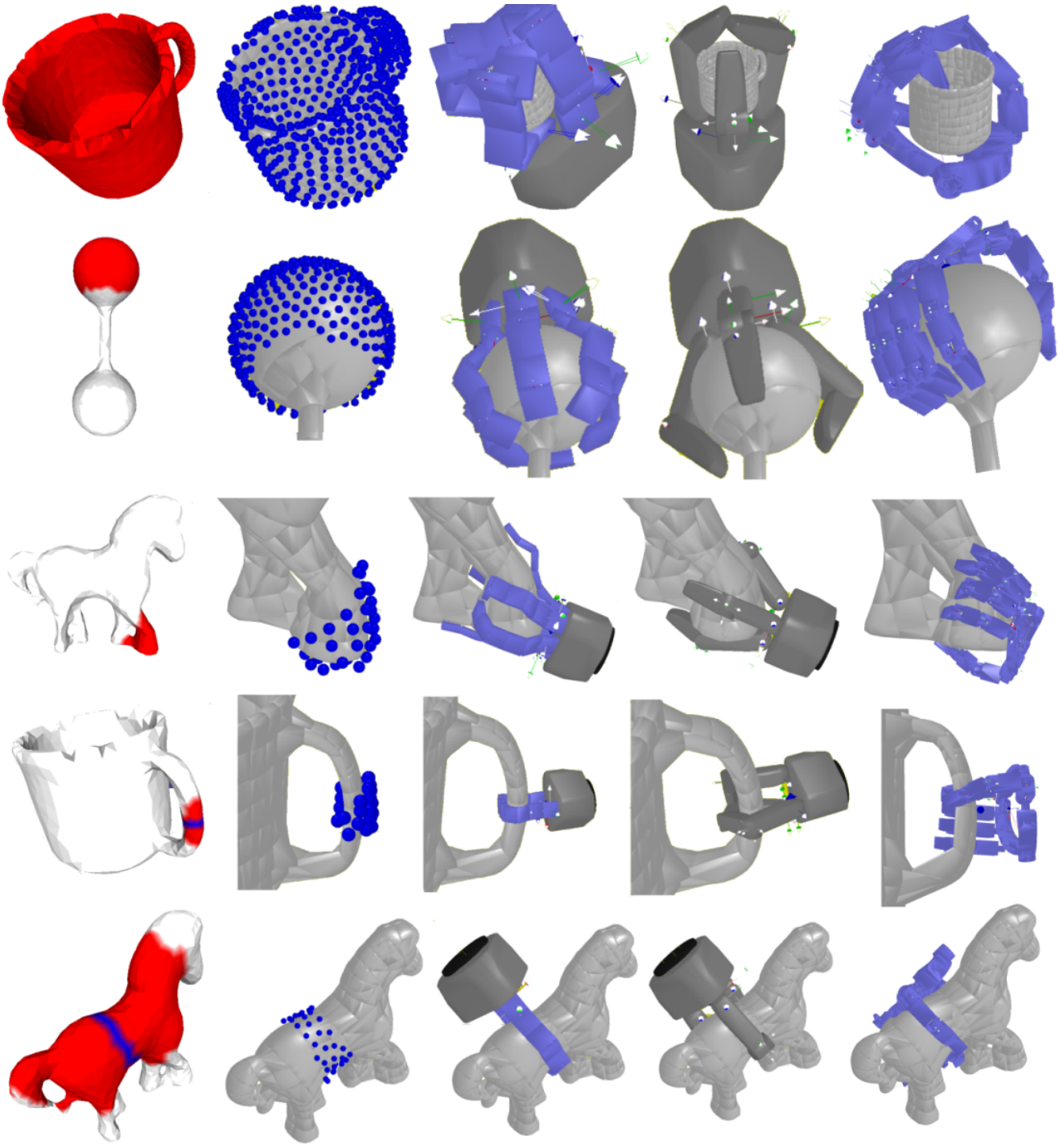

Fig. 8. We display examples of grasps generated by our method. The three top rows represent attempted $\mathbb{S}^2$ caging grasps and the lower two attempted $\mathbb{S}^1$ cages respectively. All displayed grasps apart from the grasps on the leg of the pony in the case of the net of points, the Schunk hand and the anthropomorphic hand (second, fourth and fifth column in the third row) pass our PhysX caging test. The first column shows reconstructed noisy meshes with the selected approximate geodesic ball $G_r(p)$ in red and centred at the vertex with highest $S_r(p)$ (first three objects) and highest $W_r(p)$ (lower two meshes). The edge-path $P_r(p)$ is highlighted in blue for circle cages. The other four columns demonstrate generated grasps for four types of manipulators. The topmost cup object has smallest size (scale factor of 1). The dumbbells are of medium size and the pony in the middle and the second cup are large. Finally, the last row shows generated $\mathbb{S}^1$ grasps for a medium sized pony object.

In case of $\mathbb{S}^1$ caging, the winding value was always close to 2π (full circle). Interestingly, this does not always guarantee a good performance since a cylindrical subpart might be too small or not reachable at all, preventing a good caging grasp. Nevertheless, the net of points, the anthropomorphic and the 2-finger hand have shown promising stability rates. The third finger in the case of the Schunk hand might be both beneficial (*e.g.* when the object is very small) and disadvantageous (*e.g.* due to collisions).

In summary, the high percentages of stable grasps for the 'net of points' indicate that our proposed heuristic scoring functions can successfully generate such grasps. However, differing robotic hands are not equally well suited for $\mathbb{S}^1$ and $\mathbb{S}^2$ cages as can be seen from Table I.

C. Qualitative discussion

Figure 8 displays some of the highest scoring geodesic balls together with corresponding generated grasps for several examples. The first cup object has smallest scale and can thus be fully covered by all manipulators. Since all $G_r(p)$ in this case have the same integrated curvature (*e.g.* zero for the original cup mesh), the first vertex in the list of vertices for this mesh is chosen to be the central vertex p of $G_r(p)$. The synthesized grasps for the medium size dumbbells object (integrated value of $3\pi \pm 0.16\pi$) also appeared to be stable. The last two examples show the robust behaviour of the generated cages for large and medium size objects in the case of $\mathbb{S}^1$ caging. The evaluation of some of these caging grasps is presented in the supplementary video.

VI. Conclusion

In this work, we have proposed and evaluated two new caging synthesis methods which we call circle and sphere caging. We have developed heuristic scoring functions for both caging types which allow us to identify robust caging grasps on complex 3D objects. Our approach is based on a novel geodesic ball representation of the hand-object interaction. We evaluated our proposed methods using a realistic physics simulation, with respect to robustness under simulated sensor noise and with respect to various object sizes and types of manipulators.

Our geodesic ball approach represents an approximation of the 'hand-local' geometry and is, to some extent, independent of the exact kinematic structure of the robotic hand. In future, we would like to investigate more elaborate approximations and investigate an implementation of our approach using several robot hands suitable for applying such caging grasps. Our method might be particularly interesting to combine with soft robotic actuators (e.g. created in laboratories [24], [25], and [22]).

Another potential approach could be to investigate further semi-global characteristics of a surface and to develop further methods which lead to robust caging grasps. For example, a combination of $\mathbb{S}^1$ and $\mathbb{S}^2$ scoring functions with reachability constraints could be a possible future direction.

References

[1] C. Ferrari and J. Canny, "Planning optimal grasps," *IEEE ICRA*, pp. 2290–2295, 1992.

[2] A. T. Miller and P. K. Allen, "Graspit!: A versatile simulator for robotic grasping," *IEEE Robotics and Automation Magazine*, vol. 11, pp. 110–122, 2004.

[3] B. León, S. Ulbrich, R. Diankov, G. Puche, M. Przybylski, A. Morales, T. Asfour, S. Moisio, J. Bohg, J. Kuffner, and R. Dillmann, "Opengrasp: a toolkit for robot grasping simulation," in *Proc. of the second international conference on simulation, modeling, and programming for autonomous robots*, ser. SIMPAR'10, 2010, pp. 109–120.

[4] C. Borst, M. Fischer, and G. Hirzinger, "Grasping the dice by dicing the grasp," in *IEEE/RSJ IROS*, 2003, pp. 3692–3697.

[5] J.-P. Saut and D. Sidobre, "Efficient models for grasp planning with a multi-fingered hand." *Robotics and Autonomous Systems*, vol. 60, no. 3, pp. 347–357, 2012.

[6] E. Rimon and J. W. Burdick, "Mobility of Bodies in Contact - I: A New 2nd Order Mobility Index for Multiple-Finger Grasps," 1994.

[7] A. Rodriguez, M. T. Mason, and S. Ferry, "From caging to grasping." *I. J. Robotic Res.*, vol. 31, no. 7, pp. 886–900, 2012.

[8] R. Diankov, S. Srinivasa, D. Ferguson, and J. Kuffner, "Manipulation planning with caging grasps," in *2008 IEEE International Conference on Humanoid Robots*, December 2008.

[9] J. A. Stork, F. T. Pokorny, and D. Kragic, "Integrated motion and clasp planning with virtual linking," in *IEEE/RSJ IROS*, 2013.

[10] B. Calli, M. Wisse, and P. Jonker, "Grasping of unknown objects via curvature maximization using active vision." in *IEEE/RSJ IROS*, 2011, pp. 995–1001.

[11] S. El-Khoury and A. Sahbani, "A new strategy combining empirical and analytical approaches for grasping unknown 3d objects," *Robotics and Autonomous Systems*, vol. 58, no. 5, pp. 497 – 507, 2010.

[12] K. Polthier and M. Schmies, "Straightest geodesics on polyhedral surfaces," in *ACM SIGGRAPH 2006 Courses*, ser. SIGGRAPH '06. New York, NY, USA: ACM, 2006, pp. 30–38.

[13] Y. G. Reshetnyak, *Geometry IV: Non-regular Riemannian Geometry*, ser. Encyclopaedia of Mathematical Sciences. Springer, 1993.

[14] M. Meyer, M. Desbrun, P. Schröder, and A. H. Barr, "Discrete differential-geometry operators for triangulated 2-manifolds," 2002.

[15] D. Zarubin, V. Ivan, M. Toussaint, T. Komura, and S. Vijayakumar, "Hierarchical motion planning in topological representations." in *Robotics: Science and Systems*, 2012.

[16] S. L. H. Edmond and T. Komura, "Character motion synthesis by topology coordinates," in *Computer Graphics Forum (Proc. Eurographics 2009)*, vol. 28, no. 2, Munich, Germany, 2009.

[17] M. Vahedi and A. F. van der Stappen, "On the complexity of the set of three-finger caging grasps of convex polygons," in *Robotics: Science and Systems*, 2009.

[18] T. Asfour, K. Regenstein, P. Azad, J. Schröder, A. Bierbaum, N. Vahrenkamp, and R. Dillmann, "ARMAR-III: An Integrated Humanoid Platform for Sensory-Motor Control," in *IEEE/RAS Int. Conf. on Humanoid Robots (Humanoids)*, 2006, pp. 169–175.

[19] S. Fuhrmann, J. Ackermann, T. Kalbe, and M. Goesele, "Direct resampling for isotropic surface remeshing." in *VMV*, R. Koch, A. Kolb, and C. Rezk-Salama, Eds. Eurographics Association, pp. 9–16.

[20] NVIDIA PhysX, "http://www.geforce.com," 2012.

[21] J. W. Ratcliff, "http://code.google.com/p/convexdecomposition/," 2009.

[22] E. Brown, N. Rodenberg, J. Amend, A. Mozeika, E. Steltz, M. R. Zakin, H. Lipson, and H. M. Jaeger, "Universal robotic gripper based on the jamming of granular material," *Proceedings of the National Academy of Sciences*, vol. 107, no. 44, pp. 18 809–18 814, Oct. 2010.

[23] M. Toussaint, "libors: Open robot simulation toolkit, http://ipvs.informatik.uni-stuttgart.de/mlr/marc/source-code/," 2012.

[24] R. Deimel and O. Brock, "A compliant hand based on a novel pneumatic actuator," in *IEEE ICRA*, 2013.

[25] F. Ilievski, A. D. Mazzeo, R. F. Shepherd, X. Chen, and G. M. Whitesides, "Soft robotics for chemists," *Angew Chem Int Ed Engl*, vol. 50, 2011.

[26] G. Wei, J. Dai, S. Wang, and H. Luo, "Kinematic analysis and prototype of a metamorphic anthropomorphic hand with a reconfigurable palm," *International Journal Of Humanoid Robotics*, vol. 8, no. 3, pp. 459 – 479, 2011.

[27] P. Cignoni, M. Corsini, and G. Ranzuglia, "Meshlab: an open-source 3d mesh processing system," *ERCIM News*, no. 73, pp. 45–46, April 2008.